Available online at www.sciencedirect.com
SCIENCE DIRECT
Journal of Catalysis 234 (2005) 496–508
JOURNAL OF CATALYSIS
www.elsevier.com/locate/jcat

Deactivation characteristics of lanthanide-promoted sol–gel Ni/Al_2O_3 catalysts in propane steam reforming

Sittichai Natesakhawat, Rick B. Watson, Xueqin Wang, Umit S. Ozkan *

The Ohio State University, Department of Chemical and Biomolecular Engineering, 140 W. 19th Avenue, Columbus, OH 43210, USA

Received 26 April 2005; revised 9 July 2005; accepted 11 July 2005

Available online 11 August 2005

Abstract

Lanthanide-promoted sol–gel nickel catalysts supported on alumina were studied with regard to their activity and stability for propane steam reforming. X-Ray photoelectron spectroscopy, in situ X-ray diffraction, temperature-programmed oxidation, transmission electron microscopy, thermogravimetric analysis coupled with temperature-programmed reaction, and sequential temperature-programmed coking/gasification/hydrogenation were used to investigate the deactivation characteristics of the catalysts prepared. Adding small amounts (2 wt%) of lanthanide elements (i.e., La, Ce, and Yb) significantly improves steam reforming activity and stability. Although the catalysts deactivate more rapidly at higher reaction temperature, the activity loss can be suppressed by increasing the H_2O/C ratio. The catalyst deactivation can be attributed to a combination of nickel sintering and coke formation. In addition, there appears to be partial oxidation of metallic sites after exposure to the reaction medium. Lanthanides cause enhanced sintering resistance, leading to smaller nickel crystallites in Ni/Al_2O_3 catalysts. Cerium promotion effectively inhibits coking by increasing active oxygen species on the nickel surface due to enhanced water adsorption and gasification. Incorporation of cerium also reduces the dissolution and diffusion of carbon through nickel particles, thus preventing the formation of carbon filaments.

Keywords: Nickel; Lanthanides; Ceria; Sol–gel; Steam reforming; Hydrogen; Deactivation; Sintering; Coke formation; Gasification

1. Introduction

Interest in steam reforming (SR) of hydrocarbons has been increasing, due to the need for efficient and cost-effective reforming technologies for hydrogen production in fuel cell applications. In practice, SR of hydrocarbons, especially methane, is performed at high temperatures over Ni-based catalysts. However, the high temperature required may favor several routes of formation of carbon deposits, including the Boudouard reaction and methane/hydrocarbon decomposition. In addition, Ni catalysts tend to agglomerate and then lose their active surface area under SR conditions, resulting in short catalyst lifetimes. Consequently, novel preparation and promotion techniques that can resist rapid catalyst deactivation by coking and sintering are essential.

Much effort has focused in developing Ni catalysts with improved resistance to coke formation by adding promoters. Alkali metals, such as K_2O and CaO, have been shown to improve coking resistance by enhancing carbon gasification but at the cost of reduced catalytic activity [1,2]. Introducing small amounts of molybdenum or tungsten (0.5 wt% MoO_3 or WO_3) into Ni catalysts has been shown to increase coking resistance with no decrease in catalytic activity [3–7]. The following mechanism for coke minimization on molybdenum-promoted Ni catalysts was proposed: Mo^{n+} on the nickel surface is first oxidized to $Mo^{(n+2)+}$, which then reacts with adsorbed Ni–C or Ni–CH_x yielding CO and H_2, and is finally reduced back to Mo^{n+} [6].

Alternatively, lanthanides appear to be promising promoters, because they can inhibit coke formation without sacrificing catalytic activity [8–10]. Zhuang et al. [8] investigated

* Corresponding author. Fax: +1-614-292-3769.
E-mail address: ozkan.1@osu.edu (U.S. Ozkan).

0021-9517/$ – see front matter
doi:10.1016/j.jcat.2005.07.014

the effect of cerium oxide as the promoter in $MgAl_2O_4$-supported Ni catalysts for methane SR at 550 °C. Cerium promotion showed a beneficial effect by both decreasing the rate of carbon deposition and increasing the catalytic activity. Wang and Lu [9] reported that adding CeO_2 into Ni/γ-Al_2O_3 catalysts enhanced the nickel dispersion and reactivity of carbon deposits, leading to improved catalytic activity and stability in carbon dioxide reforming of methane. Increasing sintering resistance by adding lanthanides into supported Ni catalysts also has been reported [11,12]. Incorporation of lanthanides (4 wt%) suppressed the growth of Ni crystallites and the formation of inactive NiO and $NiAl_2O_4$ phases [11]. Furthermore, oxides of heavy lanthanides (Gd, Er, and Dy) exhibited a more pronounced effect than those of light ones (La, Pr, Nd). Teixeira and Giudici [12] suggested that the sintering rate of small nickel crystallites, particularly for narrow initial crystallite size distributions and high initial dispersions in coprecipitated Ni/Al_2O_3 catalysts, was facilitated at high temperatures in the presence of steam. However, the growth of nickel crystallites under reduction and reaction conditions could be inhibited by lanthanum promotion.

In earlier work we presented the catalytic performance of sol–gel Ni/Al_2O_3 catalysts promoted with lanthanide elements [lanthanum (La), cerium (Ce), and ytterbium (Yb)] for SR of propane [13]. In this paper we present the deactivation characteristics of these catalysts, studied using X-ray photoelectron spectroscopy (XPS), in situ X-ray diffraction (XRD), temperature-programmed oxidation (TPO), transmission electron microscopy (TEM), thermogravimetric analysis–temperature-programmed reaction (TGA-TPR), and sequential temperature-programmed coking/gasification/hydrogenation. Based on the information obtained from these studies, we then discuss possible deactivation mechanisms of lanthanide-promoted sol–gel Ni/Al_2O_3 catalysts in propane SR.

2. Experimental

2.1. Catalyst preparation

Ni/Al_2O_3 catalysts promoted with lanthanide elements (La, Ce, and Yb) were prepared using a modified sol–gel technique. The nickel and lanthanide precursors (Aldrich) used were in nitrate form. For the aluminum precursor, aluminum tri-*sec*-butoxide (ATB; Aldrich) was used. Ethanol (Alfa Aesar; 130 cm^3) was used as the solvent. The following sol–gel variables were controlled during the synthesis: nickel content, 20 wt%; lanthanide content, 2 wt%; H_2O/ATB molar ratio, 3.6; and pH of the resulting gels, 4.8. First, ATB was placed in ethanol and stirred. Then the aqueous solutions with the desired amounts of lanthanide and nickel were added dropwise into the suspension using a syringe pump at a flow rate of 0.5 cm^3/min. The aqueous lanthanide nitrate solution was added first, followed by the nickel solution. The pH of the resulting green gels was measured and adjusted by adding HNO_3 (Fisher) or NH_4OH (Fisher). The gels were stirred for an additional 15 min and then kept at room temperature for 30 min. The samples were then dried overnight in the oven at 110 °C to remove remaining water and ethanol. The dry samples were ground to a fine powder and calcined under O_2 at 450 °C (ramp rate, 10 °C/min) for 4 h.

2.2. Catalyst characterization

BET surface areas of calcined catalysts were measured by N_2 adsorption–desorption at 77 K using a Micromeritics ASAP 2010 instrument. Before measurement, the samples were degassed under vacuum at 130 °C overnight. XPS of reduced and post-reaction catalysts was performed with an AXIS Ultra XPS spectrometer with an Al anode operated at 14 kV and 10 mA. Reduction was performed with 20% H_2/N_2 at 600 °C for 2 h. Post-reaction samples collected after 20 h of propane SR were prepared using the following reaction conditions: 500 °C, $H_2O/C = 1.3$, GHSV = 124,000 h^{-1}. The samples were transferred to an XPS chamber using an inert glove box, without exposing them to the atmosphere. Spectra were corrected using the C1*s* signal located at 284.5 eV.

XRD patterns during in situ reduction of catalysts were obtained with a Bruker D8 Advance X-ray diffractometer equipped with atmosphere and temperature control stages and using Cu-K_α radiation ($\lambda = 1.542$ Å) operated at 40 kV and 50 mA. In these experiments, XRD patterns were recorded every 50 °C with a ramp rate of 10 °C/min up to 700 °C under 5% H_2/N_2.

TEM images of post-reaction catalysts were obtained with a Tecnai TF-20 operated at 100 kV. Samples were ultrasonically dispersed in ethanol, and a couple of drops of the suspension were deposited on a standard 3-mm copper grid covered with a holey carbon film. TPO of postreaction catalysts was performed using a laboratory-made gas flow system described in detail elsewhere [14]. Initially, 50 mg of catalyst was placed in a $\frac{1}{4}$-inch-o.d. quartz U-tube reactor and heated under He (40 cm^3 (STP)/min) at 200 °C for 30 min to remove moisture followed by cooling to room temperature. Subsequently, the temperature of the catalysts was raised under 1% O_2/He [40 cm^3 (STP)/min] with a ramp rate of 10 °C/min to 800 °C and held for 5 min. The desorbed species from the catalyst surface were monitored using an HP5890-MS Engine 5989A gas chromatography-mass spectrometer (GC-MS) unit under He carrier gas.

TGA-TPR experiments were performed in a Perkin-Elmer TGA7 system. Catalysts were reduced in situ under 20% H_2/N_2 at 600 °C for 2 h, followed by cooling to 250 °C under N_2. The reaction mixture [$C_3H_8/H_2O/N_2$, 30 cm^3 (STP)/min] with H_2O/C molar ratios ranging from 0.1 to 0.3 was subsequently introduced to the reduced catalysts. The temperature program was as follows: 1 min at 250 °C, 10 °C/min ramp rate to 750 °C, and

5 min at 750 °C. Sequential temperature-programmed coking/gasification/hydrogenation of catalysts was conducted with a Shimadzu GC-MS QP-5050. Before spectra collection, the catalysts were reduced in situ under the 20% H_2/N_2 catalyst at 600 °C for 2 h. The coking was then performed by exposing the catalysts to 2% C_3H_8/He at 500 °C for 1 h, followed by cooling to room temperature under He. Temperature-programmed gasification (TPG) experiments were initiated by raising the catalyst temperature under 2% H_2O/He with a ramp rate of 10 °C/min to 800 °C. After cooling to room temperature, temperature-programmed hydrogenation (TPH) experiments were performed with 10% H_2/He. TPH profiles were collected while heating the catalysts with a ramp rate of 10 °C/min to 800 °C.

2.3. Reaction studies

The steady-state reaction experiments were performed using a fixed-bed flow stainless steel reactor ($\frac{1}{4}$ inch o.d.). The reaction conditions were as follows: 500–550 °C, $H_2O/C = 1.3$–2.7, and GHSV = 124,000–248,000 h^{-1}. Before the reaction, catalysts were reduced in situ under 20% H_2/N_2 [50 cm^3 (STP)/min] at 600 °C for 2 h. The feed stream consisted of C_3H_8, H_2O, and N_2 as a diluent. The effluent from the reactor was analyzed using an automated Shimadzu GC-14A equipped with flame ionization and thermal conductivity detectors. Separations were performed under Ar using two columns, a Porapak Q (12 ft × $\frac{1}{8}$ inch, stainless steel, 80/100 mesh) and Molecular Sieve 13X (5 ft × $\frac{1}{8}$ inch stainless steel, 60/80 mesh). A GOW-MAC 069-50 ruthenium methanizer operated at 350 °C was used with the flame ionization detector for the sensitive determination of CO as low as 10 ppm. Carbon and hydrogen balances were close to 100% (±5%). Conversion, yield, and activity loss were defined as follows:

$$\%\ C_3H_8\ \text{conversion} = (\text{mol of carbon converted}/\text{total mol of carbon in the feed}) \times 100,$$

$$\%\ H_2\ \text{yield} = (2 \times \text{mol of } H_2 \text{ produced}/\text{total mol of hydrogen in the feed}) \times 100,$$

$$\%\ \text{activity loss} = \left[1 - (\%\ \text{steady-state } C_3H_8\ \text{conversion})/(\%\ \text{initial } C_3H_8\ \text{conversion})\right] \times 100.$$

3. Results and discussion

3.1. Catalytic activity and stability for propane SR

3.1.1. Effect of lanthanide addition

Lanthanide-promoted sol–gel 20% Ni/Al_2O_3 catalysts were evaluated with regard to activity and stability in propane SR at 500–550 °C. The feed percentages in these experiments were $C_3H_8/H_2O/N_2 = 1/4/95$. Propane conversion and percent activity loss data (inset) are presented in Fig. 1.

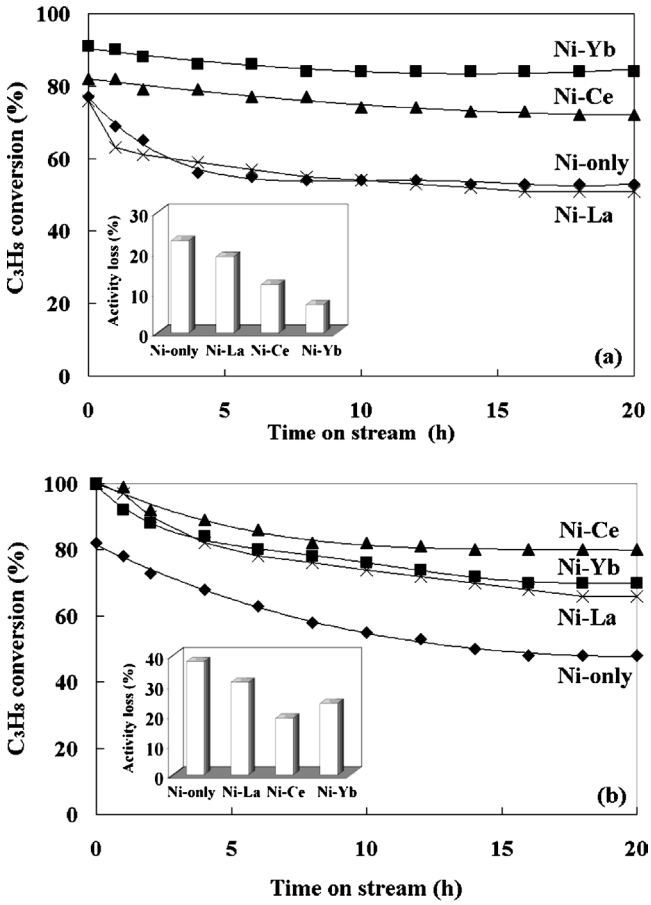

Fig. 1. C_3H_8 conversion as a function of time on stream: (a) $T = 500$ °C, $H_2O/C = 1.3$, GHSV = 124,000 h^{-1}; (b) $T = 550$ °C, $H_2O/C = 1.3$, GHSV = 186,000 h^{-1}. The activity loss of the same set of catalysts is shown as insets.

To ensure that the system did not approach equilibrium-limited regime, GHSV was increased at higher temperatures. As shown in Fig. 1a, at 500 °C and 124,000 h^{-1}, the 20% Ni–2% Ce/Al_2O_3, and 20% Ni–2% Yb/Al_2O_3 catalysts exhibited increased propane conversion, whereas the 20% Ni–2% La/Al_2O_3 and 20% Ni/Al_2O_3 catalysts showed similar SR activity. The C-containing products from propane SR are CO, CO_2, and CH_4, with CO_2 the main product. The distribution of C-containing products is little affected by lanthanide promotion under these reaction conditions. More important, the addition of lanthanide elements leads to significantly improved catalyst stability, as evidenced by a smaller percentage of activity loss. At 500 °C, the loss of catalytic activity increases in the following order: Ni–Yb/Al_2O_3 (7%) < Ni–Ce/Al_2O_3 (12%) < Ni–La/Al_2O_3 (19%) < Ni/Al_2O_3 (23%).

Increased activity loss becomes more evident with increasing reaction temperature, possibly due to more severe catalyst deactivation by sintering and coke formation, as shown in Fig. 1b. Interestingly, the highest propane conversion is achieved with the 20% Ni–2% Yb/Al_2O_3 catalyst at 500 °C, whereas the 20% Ni–2% Ce/Al_2O_3 catalyst is the best-performing catalyst with regard to catalytic activity and stability at 550 °C. It is conceivable that a beneficial effect

of cerium addition on improved coking resistance is more pronounced at elevated temperatures, thus resulting in more stable catalysts. The use of cerium oxide as a promoter or support mixed with other metal oxides (i.e., $Ce_xZr_{1-x}O_2$) to develop high-performance catalysts for hydrogen production has been reported previously [8,9,15–19]. Significantly increased catalytic activity and stability result from enhanced reducibility and reduced carbon accumulation on the active sites due to the high oxygen storage capacity of cerium oxide.

Our TPR and H_2 chemisorption studies showed that the SR activity of sol–gel Ni/Al_2O_3 catalysts is related to catalyst reducibility and nickel surface area [13]. Adding cerium results in greater reduction of nickel species and larger nickel surface area compared with ytterbium (or lanthanum) promotion. Thus in this paper we primarily report the deactivation characteristics of sol–gel $Ni–Ce/Al_2O_3$ catalysts.

3.1.2. Effect of H_2O/C ratio

The effect of H_2O/C ratio on catalytic performance of the 20% Ni/Al_2O_3 and 20% Ni–2% Ce/Al_2O_3 catalysts in propane SR was investigated at 550 °C and 248,000 h^{-1}. The H_2O/C ratio was varied in the range of 1.3–2.7 by keeping the propane flow rate constant at 6 cm^3 (STP)/min. As shown in Fig. 2a, C_3H_8 conversion increases with increasing H_2O/C ratio. An increase in catalytic activity is more evident with the 20% Ni–2% Ce/Al_2O_3 catalyst; 47 and 99% C_3H_8 conversion were obtained at H_2O/C ratios of 1.3 and 2.7, respectively. A significant improvement in catalyst stability is apparent at higher H_2O/C ratios when cerium is present in the catalysts [Fig. 2b]. In contrast, the improved catalyst stability of the 20% Ni/Al_2O_3 catalyst is barely noticeable with increasing H_2O/C ratios. At 550 °C and $H_2O/C = 2.7$, the 20% Ni–2% Ce/Al_2O_3 catalyst lost only 1% of its initial activity (time on stream [TOS] = 1 h) after steady state was reached, whereas the 20% Ni/Al_2O_3 catalyst had a 62% activity loss. Fig. 3 shows plots of H_2 formation rate at 550 °C as a function of TOS observed with the 20% Ni/Al_2O_3 and 20% Ni–2% Ce/Al_2O_3 catalysts at different H_2O/C ratios. A decline in H_2 formation rate is seen over both catalysts at lower H_2O/C ratios, possibly due to catalyst deactivation by coke formation. At $H_2O/C = 2.7$, the 20% Ni/Al_2O_3 catalyst still exhibited a pronounced reduction in H_2 formation rate during the first 15 h, whereas the Ni–Ce catalyst exhibited very stable performance. Reaction results indicated that high H_2O/C ratio coupled with cerium promotion was very effective in enhancing catalytic activity as well as preventing activity loss.

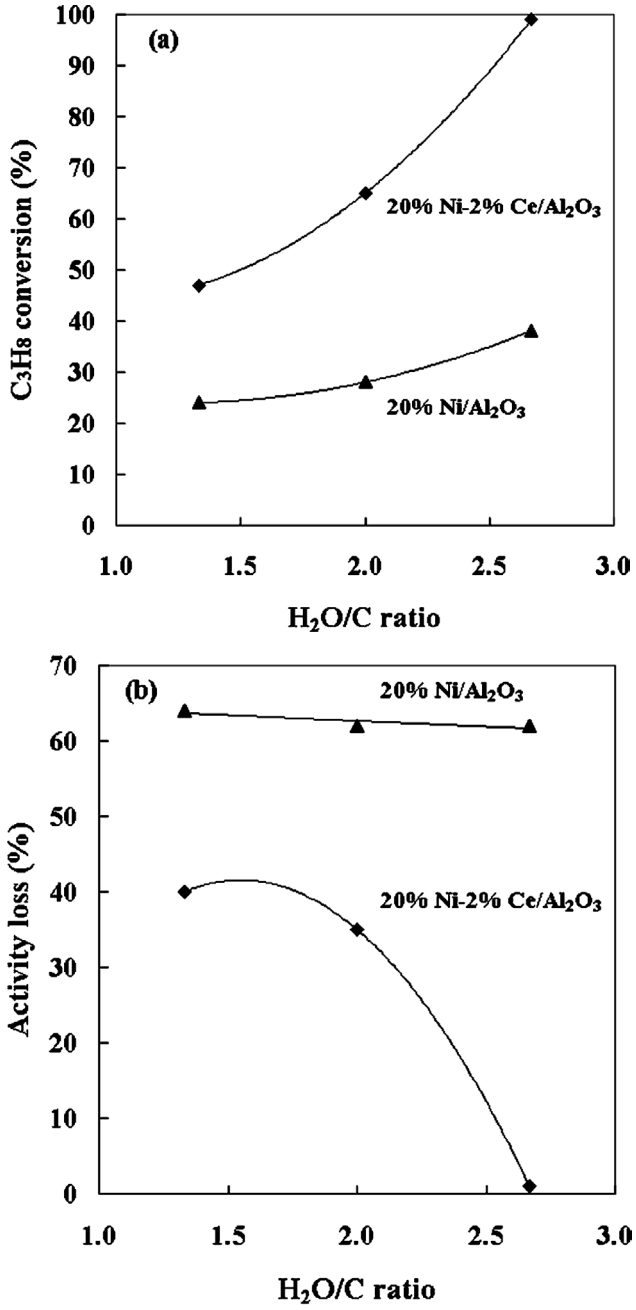

Fig. 2. Effect of H_2O/C ratio on catalytic activity and stability of 20% Ni/Al_2O_3 and 20% Ni–2% Ce/Al_2O_3 catalysts in propane steam reforming: (a) C_3H_8 conversion, (b) activity loss [reaction conditions: 550 °C, $F(C_3H_8) = 6$ cm^3 (STP)/min, GHSV = 248,000 h^{-1}].

3.2. Deactivation characteristics of sol–gel catalysts

3.2.1. Reoxidation of metallic nickel sites

Fig. 4 shows the Ni2p region of XPS of sol–gel 20% Ni/Al_2O_3 catalysts promoted with 2 wt% La, Ce, and Yb after being exposed to the propane SR reaction medium at 500 °C for 20 h. The Ni2p spectra of the catalysts exhibit features that are assigned to Ni^{2+} with Ni2$p_{3/2}$ and Ni2$p_{1/2}$ binding energies at 855.8 and 873.3 eV, respectively, and to Ni^0 with Ni2$p_{3/2}$ and Ni2$p_{1/2}$ binding energies at 852.7 and 870.2 eV, respectively [20–23]. The signal of Ni^{2+} species is likely to be due to $NiAl_2O_4$, although the possibility of a NiO phase cannot be excluded, because the Ni2p binding energies for these two species are very close together [13]. The Ni2$p_{3/2}$ signal corresponding to Ni^{2+} is accompanied by a broader peak located at 860.8 eV because of a strong shake-up process [24]. Deconvolution of the Ni2p spec-

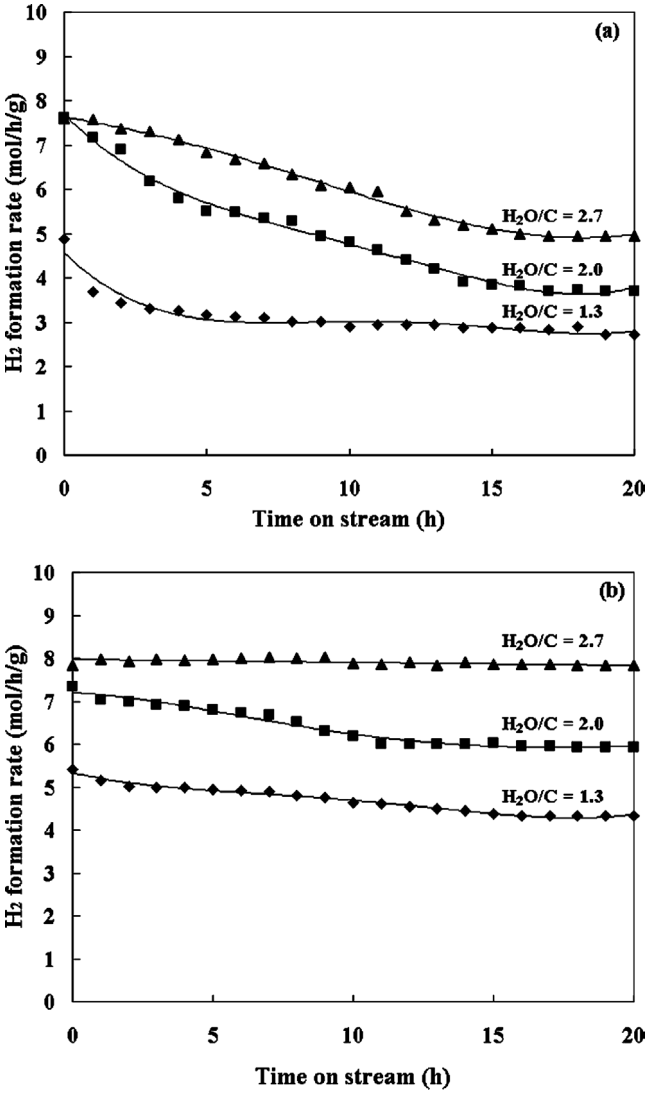

Fig. 3. H_2 formation rate at 550 °C as a function of time on stream for (a) 20% Ni/Al_2O_3 and (b) 20% Ni–2% Ce/Al_2O_3.

tra was performed by the Gaussian–Lorentzian curve-fitting method to determine the peak areas for obtaining relative surface concentrations of nickel species. The spectra were deconvoluted using the constraints of equal spin-orbit splitting of Ni2p peaks (17.5 eV), with the height ratio of Ni2$p_{3/2}$ and Ni2$p_{1/2}$ held constant at 2.0 (theoretical value) and the full width at half-maximum of these peaks being equal. The ratio of peak areas $A^0_{Ni}/(A^0_{Ni} + A^{2+}_{Ni})$ is used to illustrate the degree of reduction before and after reaction. As shown in Table 1, a decrease in $A^0_{Ni}/(A^0_{Ni} + A^{2+}_{Ni})$ ratio is seen after exposure to the propane SR atmosphere compared with freshly reduced prereaction catalysts. This is likely caused by coke deposition over Ni^0 sites. However, a partial oxidation of metallic nickel sites during the reaction cannot be ruled out, because the Ni2p binding energies for $NiAl_2O_4$ and NiO are very close. The decrease in the $A^0_{Ni}/(A^0_{Ni} + A^{2+}_{Ni})$ ratio over Ni-only catalyst (20%) is much higher than that (10–15%) over lanthanide-promoted catalysts.

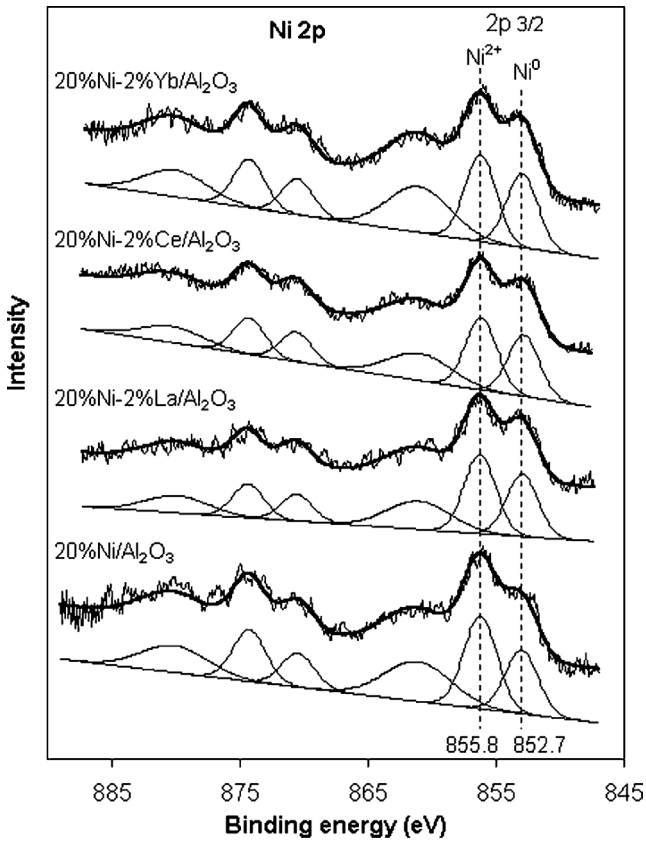

Fig. 4. Ni2p X-ray photoelectron spectra of reduced catalysts after being exposed to the propane steam reforming atmosphere at 500 °C for 20 h.

Table 1
Comparison of the ratio of XPS peak areas $A^0_{Ni}/(A^0_{Ni} + A^{2+}_{Ni})$ of the catalysts before and after 20-h propane steam reforming

Catalyst	$A^0_{Ni}/(A^0_{Ni} + A^{2+}_{Ni})$		
	Pre-reaction (reduction)	Post-reaction	Change (%)
20% Ni/Al_2O_3	0.51	0.41	−20
20% Ni–2% La/Al_2O_3	0.51	0.46	−10
20% Ni–2% Ce/Al_2O_3	0.55	0.47	−15
20% Ni–2% Yb/Al_2O_3	0.54	0.47	−13

3.2.2. Ni sintering

The sintering of Ni crystallites in lanthanide-promoted sol–gel 20% Ni/Al_2O_3 catalysts during reduction was studied from a determination of the mean Ni crystallite size by in situ XRD. The XRD patterns of the 20% Ni–2% Yb/Al_2O_3 catalyst during reduction under 5% H_2/N_2 are shown in Fig. 5. The pre-calcined catalyst is relatively amorphous, as evidenced by broad peaks at room temperature. The possible crystalline phases are NiO, $NiAl_2O_4$, and γ-Al_2O_3. No ytterbium-related crystalline phases were detected, suggesting that Yb species could be well dispersed on the alumina support or could exist within the nickel oxide matrix undetectable by XRD. As the reduction temperature is increased to 450 °C, a metallic Ni phase starts to appear. The diffraction lines of Ni(111), (200), and (220) grow in intensity with

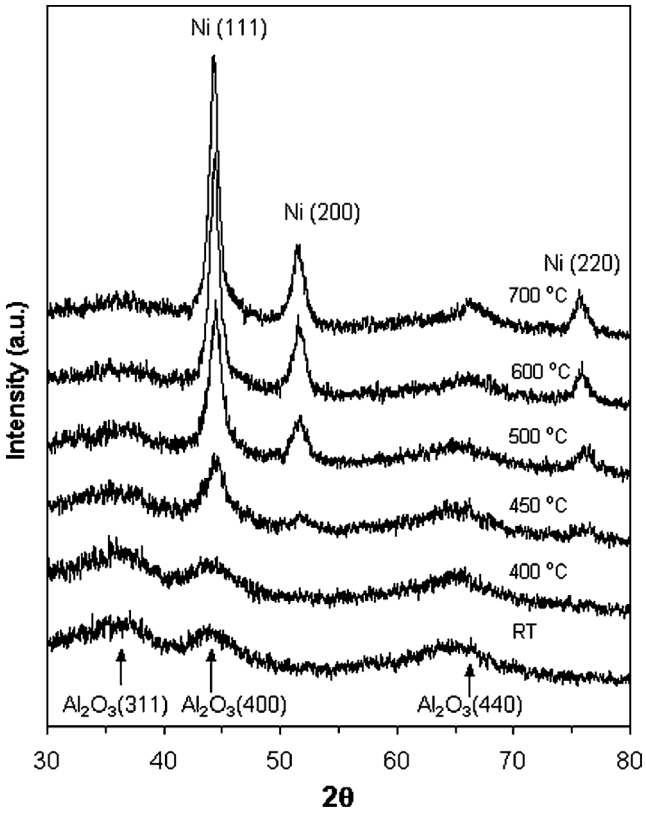

Fig. 5. In situ XRD patterns of 20% Ni–2% Yb/Al_2O_3 catalysts during reduction under 5% H_2/N_2.

Table 2
Effect of reduction temperature on nickel crystallite diameter (nm) of lanthanide-promoted sol–gel 20% Ni/Al_2O_3 catalysts

Catalyst	Reduction temperature (°C)		
	500	600	700
20% Ni/Al_2O_3	14	16	18
20% Ni–2% La/Al_2O_3	12	13	14
20% Ni–2% Ce/Al_2O_3	12	13	14
20% Ni–2% Yb/Al_2O_3	11	12	13

further increase in reduction temperature up to 700 °C. In situ XRD results indicate that high reduction temperatures (>500 °C) are necessary to reduce nickel species to a metallic state due to a strong interaction of nickel oxide with the alumina support. Nickel crystallite diameters of different lanthanide-promoted 20% Ni/Al_2O_3 catalysts were calculated from line broadening of the Ni(200) diffraction line using the Scherrer equation [25] and are listed in Table 2. Ni crystallite diameter of the catalysts increases with increasing reduction temperature. Compared with unpromoted catalyst, Ni crystallites are much smaller in lanthanide-promoted catalysts at all reduction temperatures. This suggests that the presence of lanthanide elements in sol–gel Ni/Al_2O_3 catalysts helps form smaller NiO matrices and then retards the growth of nickel crystallites during reduction.

The stabilizing effect of lanthanides to prevent Ni sintering is associated with a surface phenomenon in which lanthanides, located on the catalyst surface, could act as a "spacer" by inhibiting Ni crystallites to form larger particles during reduction. BET surface area measurements show that the addition of lanthanides results in increased surface area. The BET surface area of a freshly calcined 20% Ni/Al_2O_3 catalyst is 209 m^2/g, whereas catalysts promoted with 2% lanthanides have BET surface areas of 278–304 m^2/g. It is also possible that a substantial fraction of lanthanides could be present inside the nickel crystallites. Topsøe et al. [26] reported that the existence of strain created by the occluded Al_2O_3 phase in the iron lattice led to a shift of the equilibrium iron particle size toward smaller particles, and as a result, the presence of alumina in ammonia-synthesis iron catalysts inhibited the growth of iron particles. Similarly, lanthanides could also cause strain in the nickel lattice, which is subsequently responsible for the formation of smaller nickel crystallites after reduction. Fig. 6 displays the XRD patterns of the 20% Ni/Al_2O_3 and 20% Ni–2% Ce/Al_2O_3 catalysts reduced at 700 °C. α-Al_2O_3 was used as an internal standard to investigate a change in the lattice parameter of the metallic Ni phase when cerium is added in sol–gel 20% Ni/Al_2O_3 catalysts. The peak maxima of Ni(111) and (200) diffraction lines of the 20% Ni–2% Ce/Al_2O_3 catalyst shift to lower diffraction angles (2θ) than those of the unpromoted sample. The calculated lattice parameters are 3.5239 Å in the 20% Ni/Al_2O_3 catalyst and 3.5278 Å in the 20% Ni–2% Ce/Al_2O_3 catalyst reduced at 700 °C. Note that the lattice parameter of pure nickel, obtained from the ICDD PDF database (PDF 4-850), is 3.5238 Å. This suggests that cerium could be embedded in the nickel lattice, thus preventing the growth of Ni crystallites.

It is known that sintering is an important cause of deactivation of Ni-based catalysts under SR conditions. The sintering process can be affected by many parameters, including temperature, chemical environment, catalyst composition and structure, and support morphology [27–29]. The sintering rate of Ni crystallites was enhanced considerably by high temperature and the presence of water in the feed gas [12,30]. Type of support also plays a role in the thermal stability of active metal phase, thus affecting the sintering process. Nickel was found to be much more stable on alumina compared with silica in a hydrogen atmosphere at 700 °C, due in part to a stronger metal–support interaction for Ni/Al_2O_3 catalysts [30].

3.2.3. Coke formation

Our reaction results indicate that the introduction of lanthanide elements in sol–gel 20% Ni/Al_2O_3 catalysts significantly enhances SR activity and stability. It is likely that lanthanide promotion strongly affects the coking process under SR conditions, thus improving the catalyst resistance to coking. To investigate the nature and amount of carbonaceous species formed on the surface during reaction, TPO and TEM were performed with the 20% Ni/Al_2O_3 and 20% Ni–2% Ce/Al_2O_3 catalysts after 20 h propane SR. TGA-TPR experiments were conducted to determine the temper-

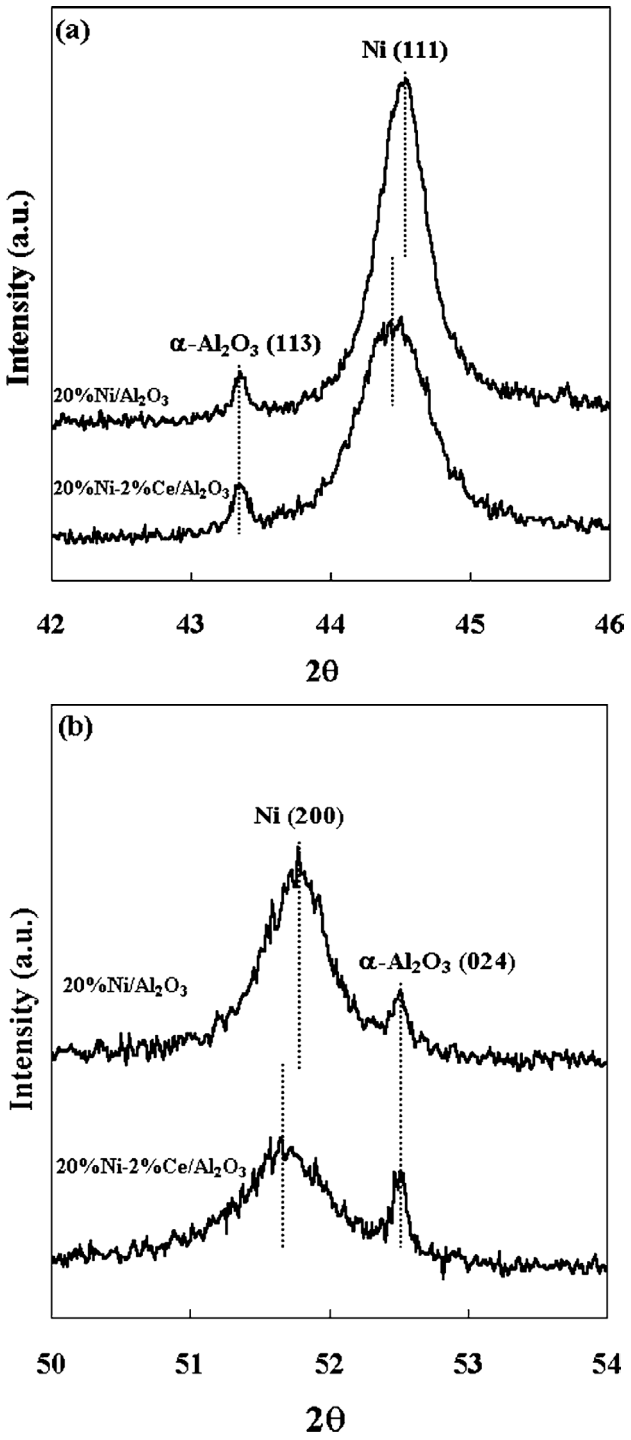

Fig. 6. Comparison of XRD patterns of 20% Ni/Al_2O_3 and 20% Ni–2% Ce/Al_2O_3 catalysts reduced at 700 °C: (a) $2\theta = 42–46°$, (b) $2\theta = 50–54°$.

ature of coking initiation. In addition, coking studies were performed using sequential temperature-programmed coking/gasification/hydrogenation experiments.

3.2.4. TPO experiments

TPO profiles of carbon deposited on the 20% Ni/Al_2O_3 and 20% Ni–2% Ce/Al_2O_3 catalysts after 20 h propane SR at 500 °C, $H_2O/C = 1.3$ are shown in Fig. 7. TPO profiles of carbon deposited on both catalysts were similar. Primarily, two peaks were observed, indicative of two types of carbonaceous species with different reactivities toward oxidation. A low-temperature peak at 360 °C can be assigned to monoatomic carbon, which is highly reactive and easily oxidized from the nickel surface [9,31–34]. A larger peak at 640 °C may be due to filamentous carbon, which is more stable and oxidizes at higher temperatures [35–37]. However, the possibility that the carbon is deposited on the alumina support, which could also be burned off at higher temperatures, cannot be ruled out. Although the temperatures at which the CO_2 is eluted from the surface were identical for the two catalysts, the amount of CO_2 evolution from the oxidation of carbon deposited on the 20% Ni/Al_2O_3 catalyst was much higher than that on the Ce-promoted catalyst, suggesting that much greater carbon deposition on Ni-only catalysts. As displayed in the inset, the amounts of carbon deposited, obtained by integrating the TPO curves, were 1.7 and 0.2 mg/m^2 on the 20% Ni/Al_2O_3 and 20% Ni–2% Ce/Al_2O_3 catalysts, respectively. The amount of carbon deposited on the catalyst was reduced by approximately 90% on cerium promotion. Furthermore, the formation of carbon filaments is markedly suppressed when cerium is present, as indicated by a lower ratio of high-temperature (640 °C) to low-temperature (360 °C) peak areas.

The effect of cerium as a promoter in coke minimization can be attributed to its unique properties as an oxygen carrier. The redox properties of ceria and the high lability of lattice oxygen are among the most important factors contributing to the catalytic reactivity of CeO_2 in oxidation reactions [38]. Under SR conditions, the presence of cerium could accelerate the reaction of steam with adsorbed species on the nickel surface [8]. Subsequently, surface carbon species are quickly converted to products, decreasing the accumulation of carbon deposits on the catalysts.

3.2.5. TEM experiments

TEM was conducted to further characterize the structure of carbon deposited on the 20% Ni/Al_2O_3 and 20% Ni–2% Ce/Al_2O_3 catalysts after 20 h propane SR at 500 °C. As shown in Fig. 8, there is clear evidence of significant amounts of carbon filaments covering nickel particles on unpromoted catalyst. Most of these filaments exhibited some degree of curvature, possibly due to an unequal diffusion of graphitic carbon through nickel particles [39]. Conversely, no carbon filaments were seen on post-reaction 20% Ni–2% Ce/Al_2O_3 catalyst. This indicates that carbon deposition is greatly suppressed by the addition of cerium in Ni/Al_2O_3 catalysts. The nickel particles remained relatively small (10–15 nm diameter) and were homogeneously distributed. The morphology of a filament obtained with the 20% Ni/Al_2O_3 catalyst is shown in Fig. 9. A nickel particle is seen at the tip of the carbon filament. Deformation of the nickel particle occurred on carbon filament formation, causing a pear-shaped appearance [40,41]. Moreover, the diameter of the carbon

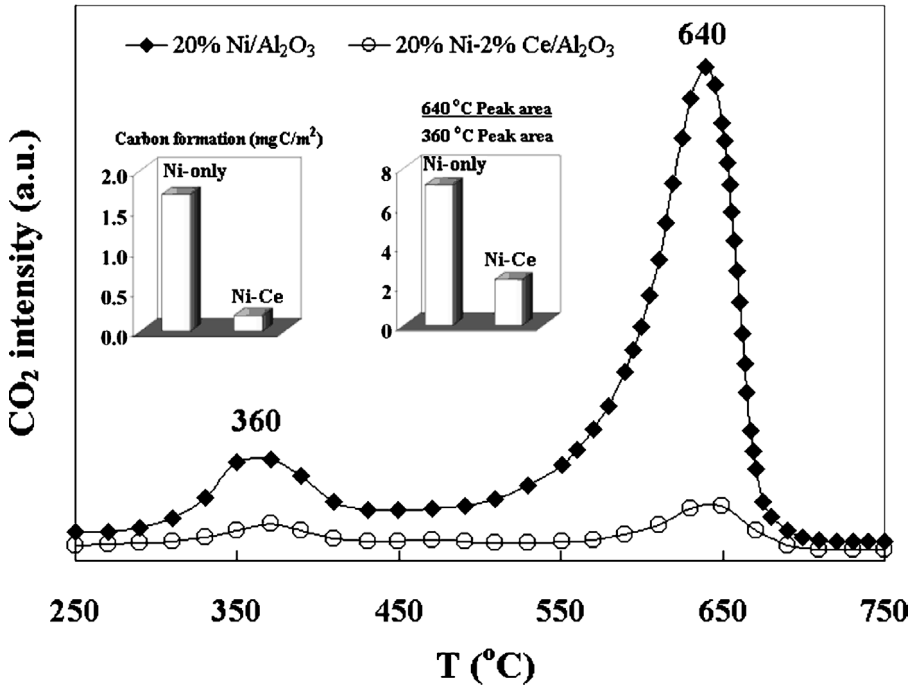

Fig. 7. TPO profiles of carbon deposited on 20% Ni/Al_2O_3 and 20% Ni–2% Ce/Al_2O_3 catalysts. Calculated carbon formation rates and ratios of 360 and 640 °C peak areas are shown as insets.

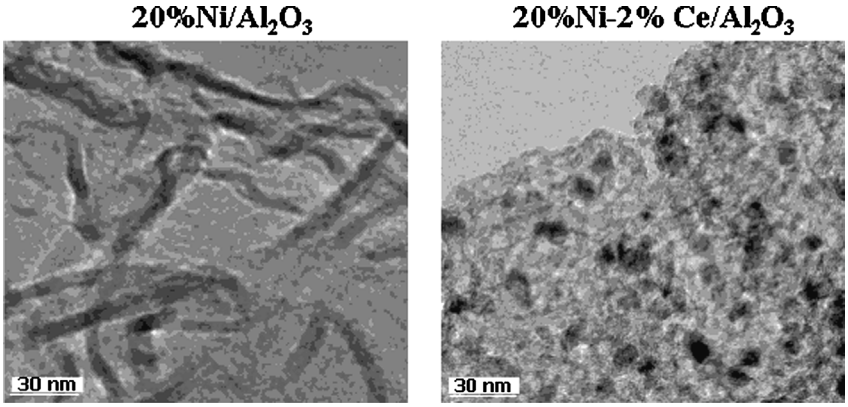

Fig. 8. TEM images of carbon deposited on catalysts after 20 h propane steam reforming over 20% Ni/Al_2O_3 and 20% Ni–2% Ce/Al_2O_3 catalysts.

filament formed on the unpromoted sample was about 8–10 nm, roughly the same as that of the Ni particle at the tip of the carbon filament. This finding suggests that the size of nickel particles determines the width of carbon filaments. The growth of carbon filaments was observed previously with nickel particle sizes in the 10–60 nm range [36]. It is intuitive that nickel particles located at the filament tips may remain immobile and not contribute to SR activity, causing rapid catalyst deactivation, as observed with the 20% Ni/Al_2O_3 catalyst. The morphology of carbon deposited on the 20% Ni–2% Ce/Al_2O_3 catalyst is quite different than that of carbon filaments formed on unpromoted catalyst. Carbon is seen to spread around a nickel particle that remains on the alumina support surface.

3.2.6. TGA-TPR experiments

As previously discussed, TPO and TEM results clearly indicate adding cerium to sol–gel 20% Ni/Al_2O_3 catalysts considerably improves resistance to coking. A TPR (i.e., SR of hydrocarbons) coupled with TGA was performed to investigate the coking resistance of Ni-based catalysts. The introduction of small amounts of MoO_3 (0.5–2 wt%) [42,43] or K_2O [44] into Ni-based catalysts was reported to increase the coking initiation temperature when steam ratio was increased, which implies improved coking resistance.

The H_2O/C ratios in TGA experiments were smaller than those used in steady-state reaction experiments, to accelerate the coking process. The effect of H_2O/C ratio on the weight changes on reduced 20% Ni/Al_2O_3 and 20% Ni–2%

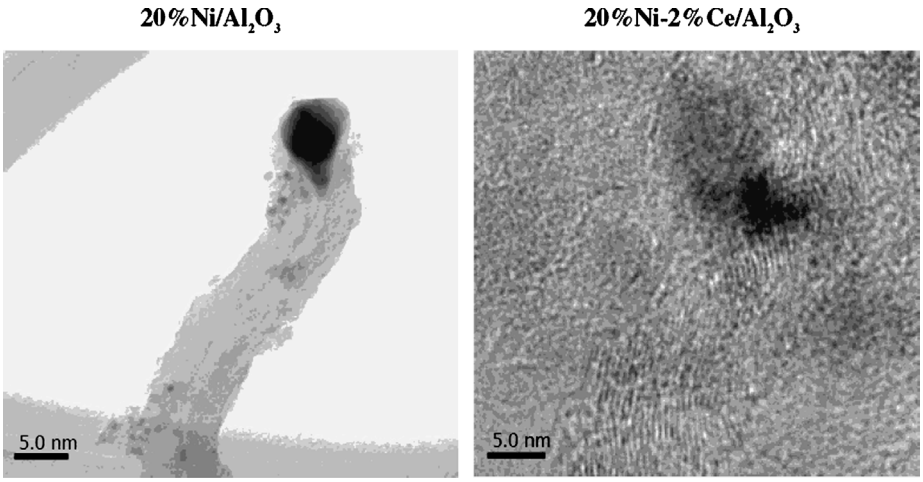

Fig. 9. The morphology of carbonaceous species on 20% Ni/Al_2O_3 and 20% Ni–2% Ce/Al_2O_3 catalysts after propane steam reforming.

Ce/Al_2O_3 catalysts during the TPR of propane with steam is shown in Fig. 10. The weight increase due to coke formation during propane SR on Ce-promoted catalyst was less pronounced than that on unpromoted catalyst at all steam ratios. At H_2O/C ratio = 0.1, a 77% weight increase was obtained with the 20% Ni–2% Ce/Al_2O_3 catalyst at 750 °C, compared with a 102% weight increase on unpromoted catalyst. The amount of carbon deposited decreased with increasing steam ratio, suggesting that more coke was gasified at higher concentrations of steam on both catalysts; moreover, an increase in steam ratio caused an increase in coking initiation temperature. As listed in Table 3, a pronounced increase in coking initiation temperature is clearly seen when cerium is present in sol–gel Ni/Al_2O_3 catalysts. In addition, the beneficial effect of cerium promotion is more evident at higher steam ratios.

3.2.7. Sequential temperature-programmed coking/gasification/hydrogenation

Initially, catalysts were exposed to 2% C_3H_8/He at 500 °C to accelerate carbon deposition as a result of hydrocarbon dissociation, forming CH_x fragments, which are coke precursors produced during propane SR. Then TPG of carbon deposited with 2% H_2O/He and TPH of the residual carbon species with 10% H_2/He were conducted. Fig. 11 shows the changes in the concentrations of various carbon-containing species in propane decomposition. Compared with the 20% Ni/Al_2O_3 catalyst, the intensity of propane increased with TOS more noticeably over the 20% Ni–2% Ce/Al_2O_3 catalyst. It appears that propane-cracking activity to form CH_x fragments was lower in Ce-promoted catalyst than in unpromoted catalyst, leading to lower accumulation of carbon species on the catalyst surface. Moreover, the formation of CH_4 and C_2 species started at approximately 3 min and increased rapidly. However, after 6 min, a decrease in CH_4 concentration was accompanied by an increase in C_2 species signal, suggesting that the catalysts gradually lose their cracking activity with TOS. In addition, CO, CO_2, and

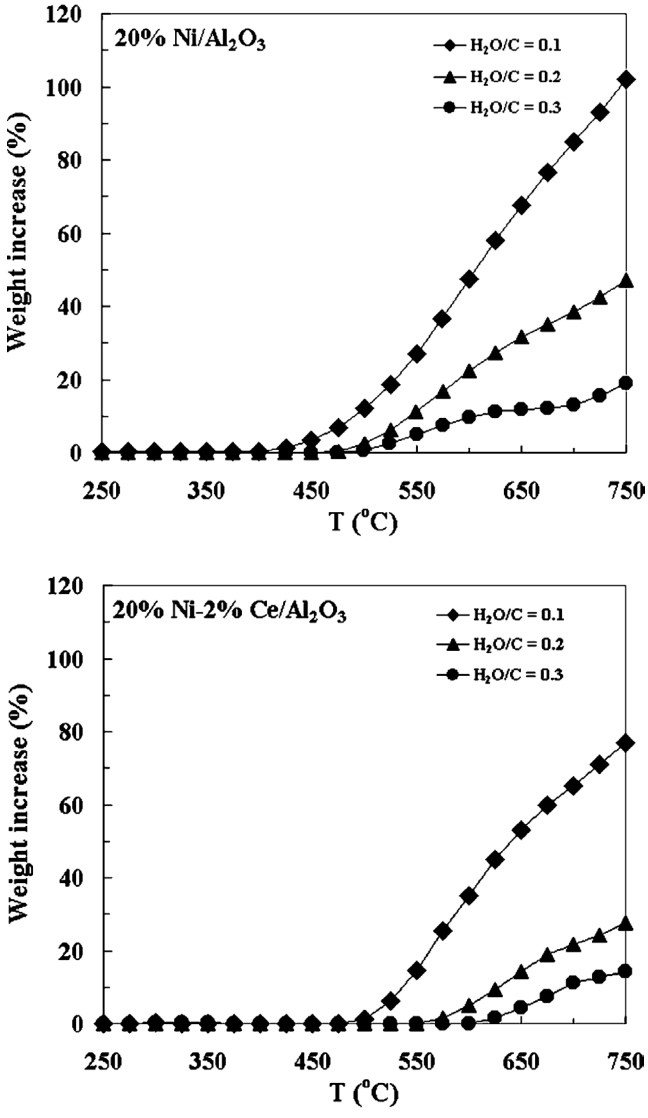

Fig. 10. Effect of steam ratio on the coking initiation temperature during propane steam reforming over 20% Ni/Al_2O_3 and 20% Ni–2% Ce/Al_2O_3 catalysts.

Table 3
Effect of steam/carbon ratio on coking initiation temperature (°C) on 20% Ni/Al_2O_3 and 20% Ni–2% Ce/Al_2O_3 catalysts

Catalyst	H_2O/C ratio		
	0.1	0.2	0.3
20% Ni/Al_2O_3	430	465	485
20% Ni–2% Ce/Al_2O_3	486	557	598

H_2O were not detected within 1 h of propane decomposition at 500 °C.

TPG profiles of carbon deposited after propane decomposition are shown in Fig. 12. It is seen that gasification of carbon deposited with 2% H_2O/He resulted in the formation of CO and CO_2. A decline in H_2O concentration is accompanied by CO and CO_2 evolution. CO_2 formation from the oxidation of carbon deposits occurs preferentially at lower temperature than CO formation. This suggests that the gasification of carbon deposits on nickel may be thermodynamically controlled. When the catalyst temperature is held at 800 °C, the intensity of CO evolution decreases, whereas the H_2O concentration rises abruptly with the presence of the CO_2 signal. The combined peak area under the CO and CO_2 evolution curves of the 20% Ni–2% Ce/Al_2O_3 catalyst is considerably smaller than that of the 20% Ni/Al_2O_3 catalyst, indicating that there is much less accumulation of carbon species from propane decomposition when cerium is present in sol–gel Ni/Al_2O_3 catalysts. In addition, a small, broad CO_2 peak is seen below 400 °C, due to the gasification of surface carbon on nickel crystallites in both catalysts. In contrast, the filamentous carbon located at the rear of nickel particles is more difficult to gasify, because it needs to diffuse back to the nickel surface. This suggests that the gasification of carbon deposits occurs on the nickel surface, as reported in the literature [45–47]. A decline in the CO signal observed with an increase in H_2O concentration at 800 °C implies that the gasification reaction is complete once the carbon species diffuse back to the nickel surface. Our results also show that back-diffusion of carbon to the nickel surface is the rate-determining step of the gasification mechanism, as reported by Trimm [48]. In case of steam gasification, H_2O is believed to dissociatively adsorb on the surface of nickel particles to form mobile surface oxygen species, which further react with carbon atoms to form CO and CO_2. Our TPG profiles show that the 20% Ni–2% Ce/Al_2O_3 catalyst exhibited a higher gasification temperature (570 °C) than the 20% Ni/Al_2O_3 catalyst (535 °C). The carbon diffusion rate possibly could be suppressed due to decreased mobility of carbonaceous species on the incorporation of cerium in nickel particles.

After the TPG experiments, the catalysts were cooled to room temperature under He. TPH experiments were then conducted with 10% H_2/He to further characterize carbon species left in the nickel crystallites after steam gasification. As displayed in Fig. 13, TPH profiles exhibited peaks of CH_4 and C_2 species over both catalysts, indicating that some

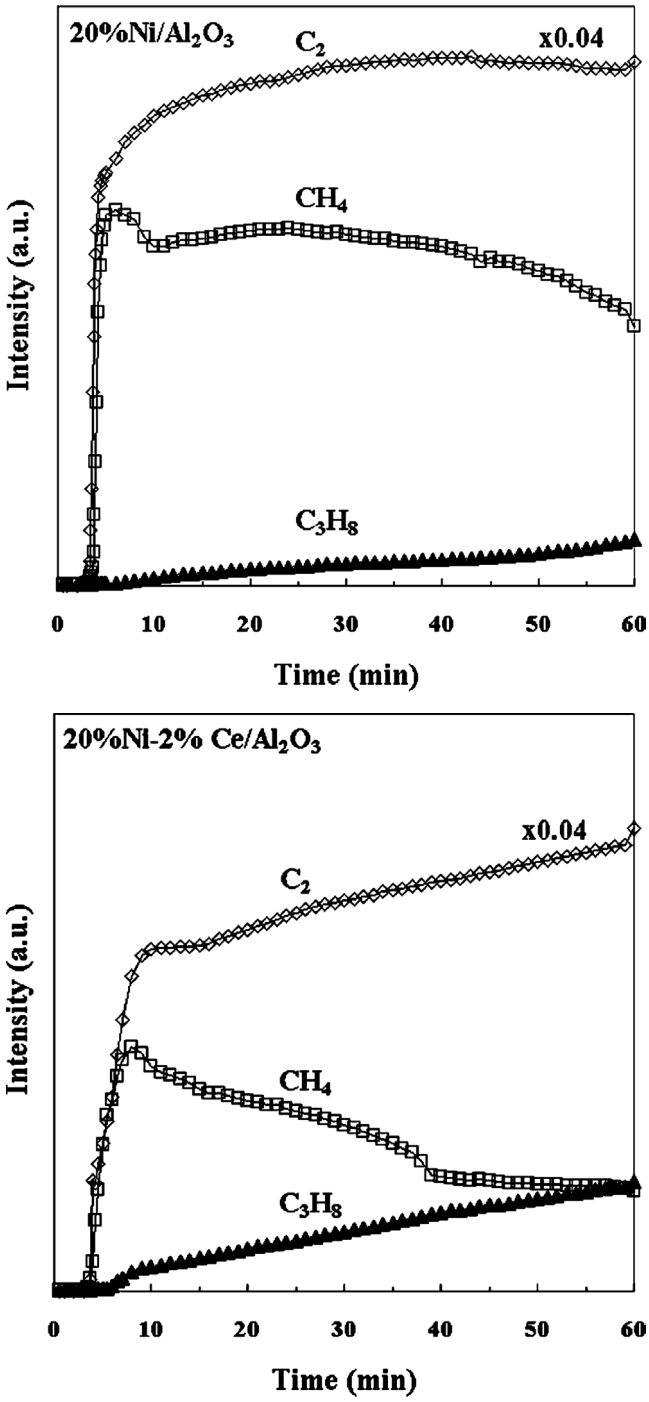

Fig. 11. Changes in the concentrations of various carbon-containing species as a function of time on stream in propane decomposition at 500 °C over 20% Ni/Al_2O_3 and 20% Ni–2% Ce/Al_2O_3 catalysts.

carbon could not completely diffuse back to the nickel surface during the gasification experiments, possibly because carbon dissolution in nickel particles had reached an equilibrium state. The hydrogenation of this "residual" carbon species started at approximately 550 °C and was complete at 800 °C on both catalysts. The peak maxima of CH_4 and C_2 species appeared at 650 and 770 °C, respectively. Furthermore, the peak area integrated under the curves of CH_4 and

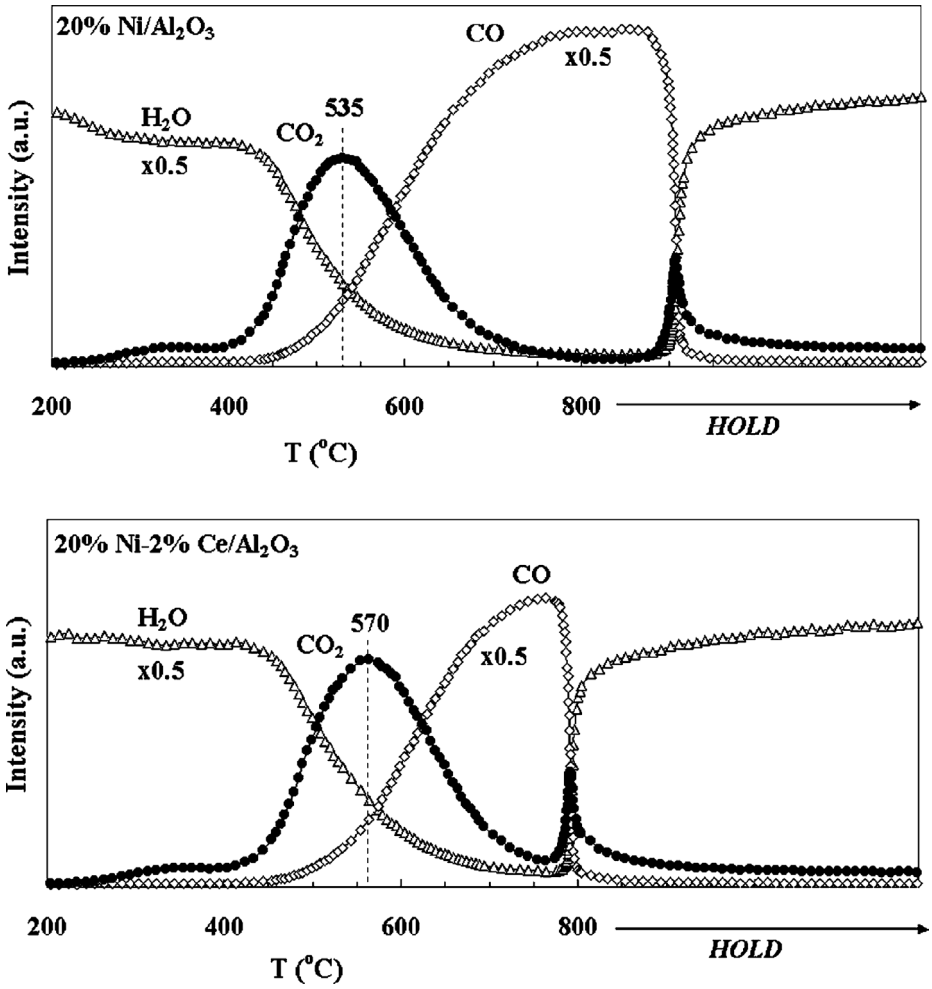

Fig. 12. TPG profiles of carbon deposited following propane decomposition.

C_2 species was lower with the 20% Ni–2% Ce/Al_2O_3 catalyst than with the 20% Ni/Al_2O_3 catalyst. The lesser amount of carbon species obtained with Ce-promoted catalyst suggests that carbon dissolution is hindered when cerium is added into nickel catalysts.

3.2.8. Coking models during SR

Based on information obtained from characterization results, coking models during propane SR over sol–gel Ni/Al_2O_3 and Ni–Ce/Al_2O_3 catalysts are proposed similar to those reported by Baker et al. [49] and Snoeck et al. [40,50]. For Ni/Al_2O_3 catalyst, the formation of carbon filaments is believed to cause rapid catalyst deactivation. The mechanism of carbon filament growth for propane SR on nickel involves various steps, including surface reactions, dissolution/segregation, carbon diffusion through nickel, and precipitation [40,49–51]. The decomposition of propane to hydrocarbon fragments (i.e., CH_x and carbon atoms) occurs initially on the nickel surface, as illustrated in Fig. 14. Carbonaceous species further dissolve and diffuse through the nickel particle, accompanied by precipitation at the rear of the nickel particle with formation of a carbon filament. The appearance of curved carbon filaments (Fig. 8) may be affected by the relative rates of nucleation of carbon filaments and of carbon diffusion through nickel, as well as the difference in diffusional path lengths on the metal–carbon interface. A pear-shaped appearance with tiny segments of nickel particle evidenced by dark spots on the filament (Fig. 9) may result from the particle deformation occurring as the carbon filament grows. Snoeck et al. [40] reported that the metal–support interaction must be overcome to lift the particle at places where no carbon extrusion occurs. Consequently, the pear shape forms as the nickel particle lifted away far from the support near the gas–metal interface.

In contrast, the addition of cerium enhances the adsorption of water, resulting in higher concentrations of active surface oxygen. The gasification of adsorbed carbon from hydrocarbon fragments on the nickel surface is so efficient that the surface carbon species can be quickly converted to products, thus decreasing the accumulation rate of carbon deposits [8]. In addition, the dissolution and diffusion of carbon species through nickel particles are greatly inhibited by the incorporation of cerium. Thus the nucleation process to form carbon filaments is retarded, due to the decreased mo-

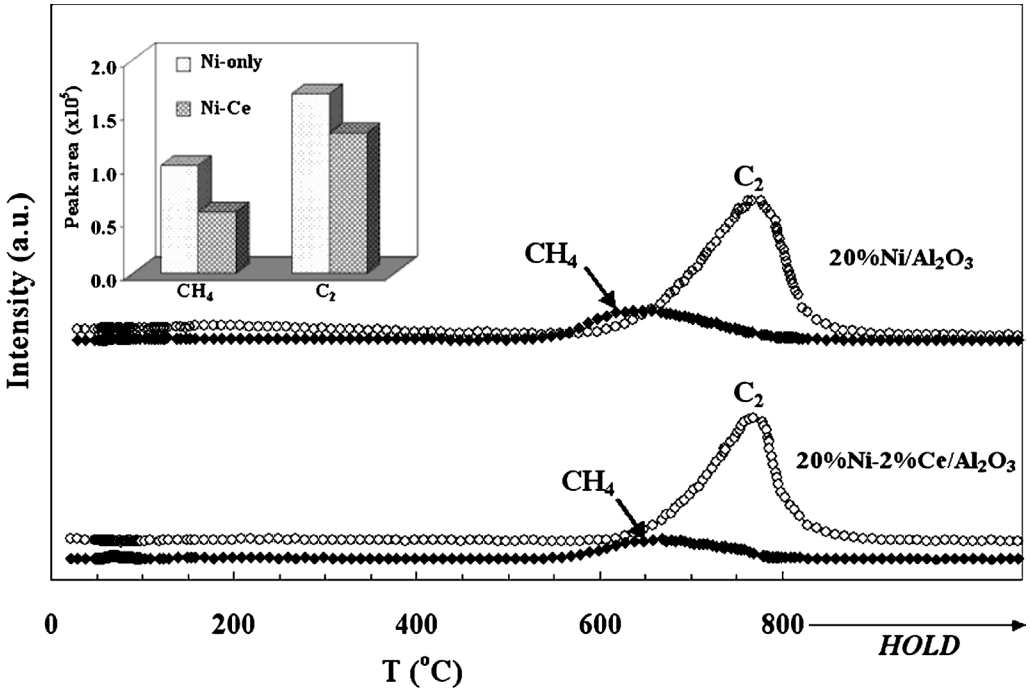

Fig. 13. TPH profiles of carbon following TPG. The inset shows the comparison of the peak area of CH_4 and C_2 species formed during TPH over 20% Ni/Al_2O_3 and 20% Ni–2% Ce/Al_2O_3 catalysts.

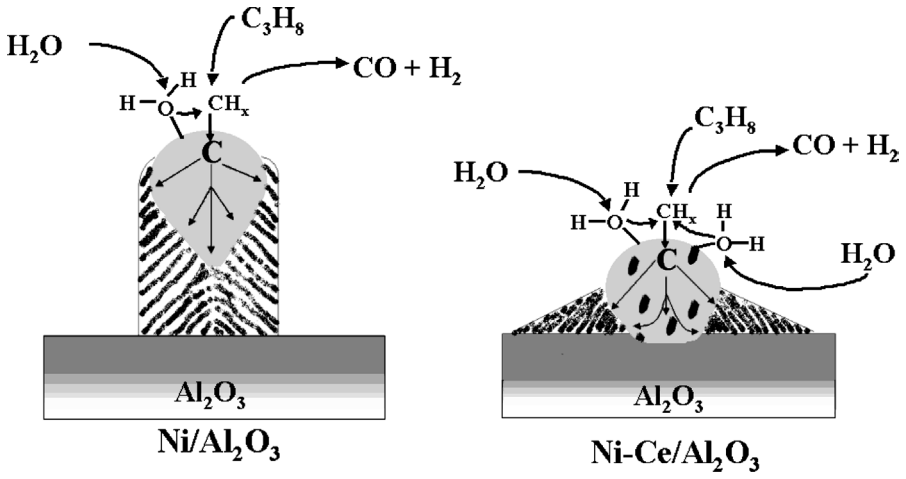

Fig. 14. Coking models during propane steam reforming over Ni/Al_2O_3 and Ni–Ce/Al_2O_3 catalysts.

bility of carbon. TEM studies detected no carbon filaments over Ni–Ce/Al_2O_3 catalyst after 20 h propane SR. Unlike Ni/Al_2O_3 catalyst, nickel particles in Ce-promoted catalyst remain on the alumina support rather than being strongly lifted far from the support. Indeed, a small amount of carbon species spreading out around nickel particles is seen with the presence of cerium, in contrast to carbon filaments of the same diameter as nickel particles.

4. Conclusions

This study has examined the effect of lanthanide promotion on catalytic performance of sol–gel nickel catalysts supported on alumina in the SR of propane. The presence of lanthanide elements (i.e., La, Ce, and Yb) was found to significantly enhance catalytic activity and stability, due in part to the fact that lanthanides help inhibit both the growth of nickel crystallites and the reoxidation of metallic nickel sites during the reaction. Coke formation is likely a major cause of deactivation, as indicated by improved catalytic activity at higher steam/carbon ratios. In particular, the catalysts promoted with cerium remain highly active and stable for 20 h when excess steam is introduced into the feed. It appears that cerium promotion greatly inhibits carbon deposition due to enhanced water adsorption and effective gasification. Furthermore, the incorporation of cerium prevents the formation

of carbon filaments by reducing the dissolution and diffusion of carbonaceous species through nickel particles.

Acknowledgments

The authors gratefully acknowledge financial support from Honda Research Institute USA, Inc. and the National Science Foundation (grant 0114098). They thank Paul H. Matter for his assistance with the TEM experiments.

References

[1] J.R. Rostrup-Nielsen, in: J.R. Anderson, M. Boudart (Eds.), Catalysis: Science and Technology, Springer, New York, 1984, p. 3.
[2] D.E. Ridler, M.V. Twigg, in: M.V. Twigg (Ed.), Catalyst Handbook, Wolfe, London, 1989, p. 225.
[3] T. Borowiecki, A. Golebiowski, Catal. Lett. 25 (1994) 309.
[4] T. Borowiecki, A. Golebiowski, B. Stasinska, Appl. Catal. A 153 (1997) 141.
[5] B. Stasinska, A. Golebiowski, T. Borowiecki, in: B. Delmon, G.F. Froment (Eds.), Catalyst Deactivation, Elsevier, Amsterdam, 1999, p. 431.
[6] T. Borowiecki, A. Machocki, in: B. Delmon, G.F. Froment (Eds.), Catalyst Deactivation, Elsevier, Amsterdam, 1999, p. 435.
[7] T. Borowiecki, G. Giecko, M. Panczyk, Appl. Catal. A 230 (2002) 85.
[8] Q. Zhuang, Y. Qin, L. Chang, Appl. Catal. 70 (1991) 1.
[9] S. Wang, G.Q. Lu, Appl. Catal. B 19 (1998) 267.
[10] R.M. Sambrook, J.R.H. Ross, US Patent 4,469,815 (1984).
[11] B.L. Su, S.D. Guo, in: B. Delmon, G.F. Froment (Eds.), Catalyst Deactivation, Elsevier, Amsterdam, 1999, p. 325.
[12] A.C.S.C. Teixeira, R. Giudici, Chem. Eng. Sci. 54 (1999) 3609.
[13] S. Natesakhawat, O. Oktar, U.S. Ozkan, J. Mol. Catal., in press.
[14] U.S. Ozkan, Y. Cai, M.W. Kumthekar, L. Zhang, J. Catal. 142 (1993) 182.
[15] S. Wang, G.Q. Lu, J. Chem. Technol. Biotechnol. 75 (2000) 589.
[16] W.S. Dong, H.S. Roh, K.W. Jun, S.E. Park, Y.S. Oh, Appl. Catal. A 226 (2002) 63.
[17] H.S. Roh, K.W. Jun, W.S. Dong, J.S. Chang, S.E. Park, Y.I. Joe, J. Mol. Catal. A 181 (2002) 137.
[18] F.B. Noronha, E.C. Fendley, R.R. Soares, W.E. Alvarez, D.E. Resasco, Chem. Eng. J. 82 (2001) 21.
[19] P. Ferreira-Aparicio, M. Benito, K. Kouachi, S. Menad, J. Catal. 231 (2005) 331.
[20] Y.J. Huang, J.A. Schwarz, J.R. Diehl, J.P. Baltrus, Appl. Catal. 36 (1988) 163.
[21] K.T. Ng, D.M. Hercules, J. Phys. Chem. A 80 (1976) 2094.
[22] J.F. Moulder, W.F. Stickle, P.E. Sobol, K.D. Bomben, Handbook of X-Ray Photoelectron Spectroscopy, Perkin–Elmer, Minnesota, 1992.
[23] A. Velon, I. Olefjord, Oxid. Met. 56 (2001) 415.
[24] X. Wang, U.S. Ozkan, J. Phys. Chem. B 109 (2005) 1882.
[25] B.D. Cullity, Elements of X-Ray Diffraction, second ed., Addison–Wesley, Massachusetts, 1978.
[26] H. Topsoe, J.A. Dumesic, M. Boudart, J. Catal. 28 (1973) 477.
[27] J. Sehested, A. Carlsson, T.V.W. Janssens, P.L. Hansen, A.K. Datye, J. Catal. 197 (2001) 200.
[28] J.R. Rostrup-Nielsen, J. Sehested, Adv. Catal. 47 (2002) 65.
[29] J. Sehested, J. Catal. 217 (2003) 417.
[30] C.H. Bartholomew, W.L. Sorensen, J. Catal. 81 (1983) 131.
[31] Z. Hou, O. Yokota, T. Tanaka, T. Yashima, Catal. Lett. 89 (2003) 121.
[32] D.L. Trimm, Catal. Today 49 (1999) 3.
[33] V.C.H. Kroll, H.M. Swaan, C. Mirodatos, J. Catal. 161 (1996) 409.
[34] L. Kepinski, B. Stasinska, T. Borowiecki, Carbon 38 (2000) 1845.
[35] S. Wang, G.Q. Lu, Ind. Eng. Chem. Res. 38 (1999) 2615.
[36] P. Wang, E. Tanebe, K. Ito, J. Jia, H. Morioka, T. Shishido, K. Takehira, Appl. Catal. A 231 (2002) 35.
[37] M.A. Goula, A.A. lemonidou, A.M. Efstathiou, J. Catal. 161 (1996) 626.
[38] A. Trovarelli, Catal. Rev. Sci. Eng. 38 (1996) 439.
[39] C. Park, M.A. Keane, J. Catal. 221 (2004) 386.
[40] J.W. Snoeck, G.F. Froment, M. Fowles, J. Catal. 169 (1997) 240.
[41] J.A. Montoya, E.R. Pascual, C. Gimon, P.D. Angel, A. Monzon, Catal. Today 63 (2000) 71.
[42] T. Borowiecki, W. Grzegorczyk, A. Denis, A. Golebiowski, Catal. Lett. 79 (2002) 119.
[43] T. Borowiecki, A. Denis, W. Grzegorczyk, A. Golebiowski, React. Kinet. Catal. Lett. 77 (2002) 163.
[44] A. Golebiowski, K. Stolecki, U. Prokop, A. Kusmierowska, T. Borowiecki, A. Denis, C. Sikorska, React. Kinet. Catal. Lett. 82 (2004) 179.
[45] J.L. Figueiredo, D.L. Trimm, J. Catal. 40 (1975) 154.
[46] J.L. Figueiredo, Carbon 19 (1981) 146.
[47] J.L. Figueiredo, Mater. Corros. 49 (1998) 373.
[48] D.L. Trimm, Catal. Rev. Sci. Eng. 16 (1977) 155.
[49] R.T.K. Baker, M.A. Barber, F.S. Feates, P.S. Harris, R.J. Waite, J. Catal. 26 (1972) 26.
[50] J.W. Snoeck, G.F. Froment, M. Fowles, J. Catal. 169 (1997) 250.
[51] J.L. Figueiredo, C.A. Bernardo, R.T.K. Baker, J. Catal. 110 (1988) 127.